Investigation of the effect of substrate orientation on the structural, electrical and optical properties of n-type GaAs$_{1-x}$Bi$_x$ layers grown by Molecular Beam Epitaxy

Sultan Alhassan[1,2,*], Daniele de Souza[3,*], Amra. Alhassni[1], Amjad. Almunyif[1] , Saud. Alotaibi[1], A. Almalki[1], M. Alhuwayz[1], Igor P. Kazakov[4], Alexey V. Klekovkin[4], Vladimir I. Tsekhosh[4], Igor A. Likhachev[5], Elkhan. M. Pashaev[5], Sergio Souto[6], Yara Galvão Gobato[3], N. Al Saqri[7], Helder Vinicius Avanço Galeti[8], Hind Albalawi[9], Nourah Alwadai[9] Mohamed Henini[1**]

[1] School of Physics and Astronomy, University of Nottingham, Nottingham NG7 2RD, UK
[2] School of Physics, College of Science, Jouf University, 74631-7365, Sakaka, Saudi Arabia
[3] Physics Department, Federal University of São Carlos, São Carlos-SP, Brazil
[4] P.N.Lebedev Physical Institute, Russian Academy of Science, 119991, GSP-1, Moscow, Russia
[5] National Research Center "Kurchatov Institute", 123182, Moscow, Russia
[6] FZEA/ZAB, University of São Paulo, Pirassununga-SP, Brazil
[7] Department of Physics, College of Science, Sultan Qaboos University, Oman
[8] Electrical Engineering Department, Federal University of São Carlos, São Carlos-SP, Brazil
[9] Department of Physics, College of Science, Princess Nourah Bint Abdulrahman University, 11671, Riyadh, Saudi Arabia

* authors contributed equally

** author contact: mohamed.henini@nottingham.ac.uk

Abstract

Current-Voltage (I-V), Capacitance-Voltage (C-V), Deep Level Transient Spectroscopy (DLTS), Laplace DLTS, Photoluminescence (PL) and Micro-Raman techniques have been employed to investigate the effect of the orientation of the substrates on the structural, electrically and optically active defects in dilute GaAs$_{1-x}$Bi$_x$ epilayers structures having a Bi composition x = ~5.4%, grown by Molecular Beam Epitaxy (MBE) on (100) and (311)B GaAs planes. X-ray diffraction results revealed that the in-plane strain in the Ga(As,Bi) layer of the samples grown on (100)-oriented substrate (-0.0484) is significantly larger than that of the samples grown on (311)B-oriented substrate. The substrate orientation is found to have a noticeable impact on the Bi incorporation and the electrical properties of dilute GaAsBi Schottky diodes. The I-V characteristics showed that (100) Schottky diodes exhibited a larger ideality factor and higher barrier height compared with (311)B samples. The DLTS measurements showed that the number of electrically active traps were different for the two GaAs substrate orientations. In particular, three and two electron traps are detected in samples grown on (100) and (311)B GaAs substrates, respectively, with activation energies ranging

from 0.12 to 0.41 eV. Additionally, one hole trap was observed only in sample grown on (100) substrates with activation energy 0.24 eV. The observed traps with small activation energies are attributed to Bi pair defects. The photoluminescence (PL) and Raman spectra have evidenced different compressive strain which affects considerably the optical properties. Furthermore, the PL spectra were also affected by different contributions of Bi- related traps which are different for different substrate orientation in agreement with DLTS results.

Keywords: dilute bismides, electrical properties, optical properties, doped semiconductor, structural disorder, defects.

1- Introduction

Dilute III-V bismide semiconductors materials such as GaAsBi alloys display strong reduction in the band gap when only a small percentage of bismuth atoms is incorporated into the lattice of the host material like GaAs which has a band gap energy of 1.424 eV at 300K. Particularly, a few percent of Bi incorporated into GaAs, i.e. $GaAs_{1-x}Bi_x$ with x being the Bi composition, leads to a giant bowing in the band gap energy (~ 88 meV/%Bi) [1], as well as an increase in spin-orbit splitting energy [2, 3]. These remarkable properties such as reduction of the band gap make GaAsBi a suitable material for several device applications such as multi-junction solar cells [4], photonic devices [1] and in long-wavelength optoelectronic devices [5].

It is well known that the growth temperature of III-V alloys can significantly influence their crystalline quality. In fact, substitutional incorporation of Bi into the host lattice of III-V compounds requires low temperature growth (< 400 °C). However, low growth temperature of GaAs causes an increased density of defects as well as leads to degradation of the optical quality of alloys [6]. For instance, growing GaAs at temperatures lower than the optimal growth temperatures (~580- 600°C) leads to the creation of many point defects, such as As-antisities (As_{Ga}), As-interstitials (As_i) and Ga vacancies [7–9]. Additionally, it is found that as the

growth temperature decreases deep level defects are generated in GaAs and their concentrations is enhanced [7, 10]. Nevertheless, using Bi as a surfactant during the growth of GaAs at low temperatures has proven to enhance surface migration, to reduce the density of defects and to suppress the formation of traps in GaAs. However, in GaAsBi epilayers where Bi is substituting an arsenic atom, Bi related defects are created. Recently, deep level transient spectroscopy (DLTS) and Laplace DLTS (LDLTS) studies of n-type $GaAs_{1-x}Bi_x$ layers grown by Molecular Beam Epitaxy (MBE) on n^+ GaAs substrates with $0 \leq x \leq 0.012$ [11] have shown that a significant reduction of the total traps concentration by a factor of ~20, in contrast to GaAs layers grown at similar temperature (~330 °C). Furthermore, as anticipated for MBE growth at this temperature, the dominant deep level defect in these layers were proposed to be an As_{Ga}-related complex defect, with a deep level energy of about 0.65 eV [11]. More recently, Ł. Gelczuk et al. [7] employed DLTS to investigate the electron deep level defects in n-type $GaAs_{1-x}Bi_x$ alloys having $0<x<0.023$ grown by MBE on conventional (100) n^+ GaAs substrates. They found that the incorporation of Bi into GaAs suppresses the formation of GaAs electron traps by reducing their total trap concentration to more than two order of magnitude compared to trap concentration in GaAs grown at similar conditions. Additionally, they reported that the two levels with activation energies ranging from 0.07 to 0.19 eV in GaAsBi with Bi compositions of 0.8%- 2.3%, are Bi- related traps. They suggested the origin of these defects to be related to Bi pair defects. [7].

Although most investigations of $GaAs_{1-x}Bi_x$ thin films and devices were performed using the conventional (100) GaAs substrates, there are few studies exploring the growth on high-index planes, which can considerably affect the Bi incorporation, and the structural, electrical and optical properties [12–16]. Remarkably, Henini et al have shown that Bi incorporation in $GaAs_{(1-x)}Bi_x$ thin films can be more enhanced by using (311)B GaAs orientation [12]. In addition, there are relatively very few researches which addressed the doping process of only

(100) $GaAs_{(1-x)}Bi_x$ [7,10,11,17–20]. Therefore, it is worth noting that the structural and optical properties of n-type $GaAs_{(1-x)}Bi_x$ alloys and devices using non-(100) GaAs substrates have not been investigated yet.

In this work the effects of substrate orientation on the structural, optical and the electrical properties of a n-type dilute $GaAs_{1-x}Bi_x$ epilayer structures grown at low temperature by MBE on conventional (100) and non-conventional (311)B n$^+$ GaAs substrates were investigated using Current-Voltage (I-V), Capacitance-Voltage (C-V), deep level defects spectroscopy (DLTS), Laplace DLTS (LDLTS), Photoluminescence (PL) and Micro- Raman techniques.

2- Experimental Details

The samples studied in this work were silicon-doped n-type $GaAs_{1-x}Bi_x$ epilayers grown on highly doped (100) and (311)B n$^+$-GaAs substrates by MBE at low temperature (~400℃). Figure 1 shows the growth of the epitaxial layers which consisted of 0.1 µm thick GaAs buffer layer heavily doped with Si with a concentration $2x10^{18}$ cm^{-3}. This was followed by 1 µm thick Si doped GaAsBi layer with a Si concentration of $2x10^{16}$ cm^{-3}. Additionally, similar structures (control samples) consisting of a 1 µm thick n-type GaAs layer (not containing Bi) were grown on (100) and (311)B GaAs substrates at similar conditions, for comparison purposes. Two n-type $GaAs_{1-x}Bi_x$ epitaxial layers with roughly 5.4% of Bi were examined (see Table 1). The compositions of the $GaAs_{1-x}Bi_x$ epilayer were measured by X-ray diffraction (XRD). For electrical characterization of these devices, all samples have been fabricated in form of circular mesas. Ge/Au/Ni/Au Ohmic contacts were thermally evaporated on the back side of the wafer, with thickness (10, 20, 20 and 150) nm, respectively. Then rapid thermal annealing (RTA) in an Ar atmosphere was performed at 380℃ for 30 seconds. This was followed by Au deposition through a shadow mask to form circular mesas Schottky contacts with different diameters on the top side of the sample. PL spectra of (100) and (311)B $GaAs_{(1-x)}Bi_x$ samples were investigated as a function of laser power and temperature using a Janis closed-loop helium

cryostat. The samples were excited with a 532 nm Nd:YAG solid state laser. The PL signal was collected in a 0.5 m Spex monochromator coupled with a nitrogen-cooled Ge detector. Micro-Raman measurements were carried out with a 633nm laser excitation. The Raman signal was measured in a Lab RAM HR Horiba Jobin Yvon system with 50x objective with spectral resolution of about 1 cm^{-1}.
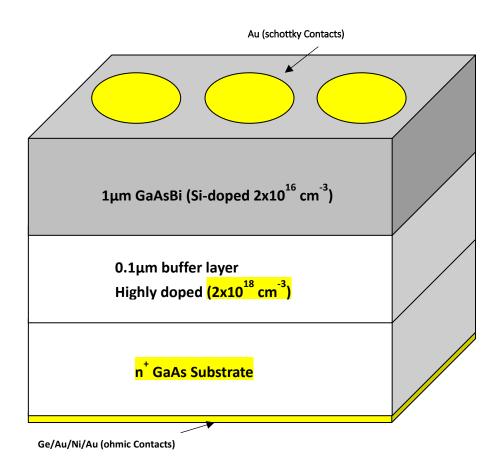
Au (schottky Contacts)

1µm GaAsBi (Si-doped 2x10^{16} cm^{-3})

0.1µm buffer layer
Highly doped (2x10^{18} cm^{-3})

n^{+} GaAs Substrate

Ge/Au/Ni/Au (ohmic Contacts)

Figure 1: Schematic diagram of n-GaAsBi grown on (100) and (311)B n^{+} GaAs substrates.

Table 1: samples details: substrate orientation, Bi content obtained from XRD and doping concentration as determined from C-V measurements.

Sample	Substrate orientation	Bi content (from XRD), %	Doping Concentration (Nd)
n-GaAs	(100)	0	3.80×10^{17} cm^{-3}
n-GaAs	(311)B	0	3.40×10^{17} cm^{-3}
n-GaAsBi	(100)	5.4	1.03×10^{16} cm^{-3}
n-GaAsBi	(311)B	5.4	1.14×10^{16} cm^{-3}

3- Results and Discussion

3.1- Structural Characteristics

X-ray diffraction measurements were carried out on a Rigaku Smartlab laboratory diffractometer in the 2θ-ω mode using Cu-K$_{\alpha 1}$ radiation and a double-crystal Ge (220) monochromator with a horizontal slit positioned in front of the detector in order to reduce diffuse and background scattering. XRD curves were measured in θ-2θ scanning mode [21]. The X-ray spot on the sample's surface was about 5mm x 0.4 mm. The structure parameters were determined from XRD curves using different (symmetrical and asymmetrical) experimental schemes. Typical XRD curves are shown in Figure 2 where symmetrical (311) and two asymmetrical (400) diffraction patterns are presented for the (311)B GaAsBi samples. Out-of-plane lattice parameter was obtained from the analysis of symmetrical XRD curves. For (100) GaAs and (311)B GaAs oriented surfaces, the asymmetric reflections (311) and (400) were measured, respectively. Asymmetrical reflexes were chosen based on the relative intensity (relationship between incident X-ray radiation and the reflected one). Asymmetrical reflections were measured from a set of planes with an angle less than the Bragg angle (θ_B) for these planes. The incidence angles θ_{asym} for these reflections are given by $\theta_{asym} = \theta_B \pm \varphi$, where

φ is the angle between asymmetrical planes and surface of the sample. Knowing the out-of-plane lattice parameter and the angle between asymmetrical reflected plane and the planes parallel to the surface of the sample, the in-plane lattice parameter of epitaxial layer $a_{//}$ can be calculated from simple geometric considerations [22].
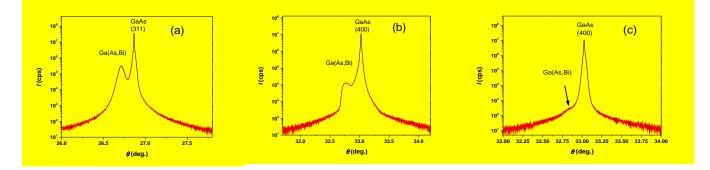

Figure 2. XRD curves of (311)B GaAsBi samples (a) symmetrical (311) diffraction pattern; (b) and (c) asymmetrical (400) diffraction patterns. Asymmetrical patterns were obtained with (b) θ_B - φ and (c) θ_B + φ incidence angles, where θ_B is the Bragg angle for the given set of crystallographic planes, and φ is the angle between (100) planes and the (311)-oriented surface.

Bi concentration was calculated from the lattice parameter of $GaAs_{(1-x)}Bi_x$ layer determined from symmetrical XRD using Vegard's law [23] with the assumption of diluted alloy of GaAs and GaBi. The drawback of such approach is that there are no reports of growth of bulk GaBi, and therefore one can only consider the theoretical calculation of GaBi lattice [24]. For the present work it was considered that GaBi has a zinc-blend cubic lattice with the lattice parameter a = 6.178 Å. It was found that Bi concentration is equal to 5.4% for both samples grown on (100) and (311)B-oriented surfaces.

Residual strains (ε_{zz} and ε_{xx}) in $GaAs_{(1-x)}Bi_x$ layer were determined from the analysis of asymmetrical XRD. Out-of-plane $a_\perp$ and in-plane strain $a_{//}$ were used to calculate the deformation of layer's lattice by using the following formulas for strains:

$$\varepsilon_{zz} = \frac{a_\perp - a_{FR}}{a_{FR}}; \varepsilon_{xx} = \frac{a_{//} - a_{FR}}{a_{FR}},$$

where $a_\perp$ is the out-of-plane lattice parameter, $a_{//}$ is the in-plane lattice parameter, and a_{FR} is lattice parameter of fully relaxed GaAs lattice. It was found that ε_{zz} is equal 0.00035 for both samples while ε_{xx} for the sample grown on (311)B-oriented surface is 2.64 times less than for (100)-oriented sample, namely -0.0484 and -0.0183 for (100) and (311)B-oriented samples, respectively.

3.2- Electrical Properties

I- Current-Voltage Characteristics

In order to select suitable diodes for DLTS and LDLTS measurements for both samples, I-V characteristics were obtained at room temperature. The reverse bias current density (J) for all samples over the voltage bias range -1V to 0V is of the order of few $\mu A/cm^2$. Typical room temperature semi-logarithmic J-V characteristics are shown in Figure 3 for all samples. It can be seen from Figure that all samples display a relatively low leakage current density. In particular, the reverse current density for samples grown on (100) is larger than that grown on (311)B. The reverse current density at bias -1V for (100) GaAs, (311)B GaAs, (100) GaAsBi and (311)B GaAsBi are 1.06×10^{-4} A/cm^{-2}, 8.26×10^{-8} A/cm^{-2} , 7.5×10^{-5} A/cm^{-2} and 6.2×10^{-6} A/cm^{-2}, respectively. The reason for the higher reverse current density in samples grown on (100) can be explained by the higher trap concentrations and more defects in (100) than (311)B [25]. Similar behaviour was observed in previous studies on n-type GaAs grown on conventional (100) and non- conventional substrate orientations (n11) [26] where the reverse current was found to decrease with increasing the index of the plane n.
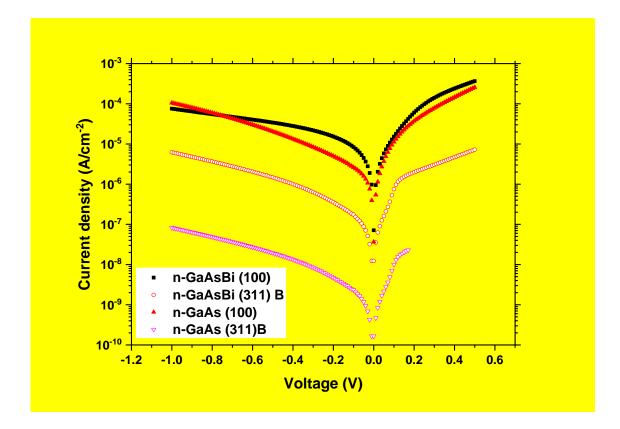
Figure 3: J-V plot for n-type (100) GaAs, (311)B GaAs, (100) GaAsBi and (311)B GaAsBi at room temperature.

Since these devices are Schottky diodes, the I-V characteristics of the diodes can be described by the thermionic emission model [27] as follows:

$$I = I_0[exp\left(\frac{q(V-IRs)}{nKT}\right) - 1] \qquad (1)$$

where q is the electronic charge, V is the applied voltage, K is the Boltzmann's constant, n is the ideality factor of the diode, T is the absolute temperature in Kelvin, Rs is the series resistance of the effective diode, and I_0 is the saturation current which is given by:

$$I_0 = AA^*T^2 \ exp\left(\frac{-q\phi_b}{KT}\right) \qquad (2)$$

where A is the diode area, A^* is the effective Richardson's constant ($A^* = 8.16$ Acm^{-2} K^{-2}), and ϕ_b is the barrier height [28].

The characteristics parameters of these devices such as (n, Rs, ϕ_b and I_0) were calculated by using the Werner's method [29].

Series resistance, ideality factors and barrier height for all the samples are obtained from the forward I-V characteristics at room temperature. These parameters are summarized in Table2.

Table 2: Experimental data of ideality factor, barrier height and series resistance, obtained from I-V characteristics at room temperature for n-type (100) GaAs, (311)B GaAs, (100) (GaAsBi) and (311)B GaAsBi.

Sample	n	φ_B (eV)	R_S (kΩ)
n-GaAs (100)	1.50±0.02	0.74±0.03	0.23±0.02
n-GaAs (311)B	1.49±0.02	0.69±0.02	1.32±0.03
n-GaAsBi (100)	2.33±0.01	0.67±0.01	36.30±0.01
n-GaAsBi (311)B	1.61±0.01	0.62±0.01	2.30±0.03

Figure 4 shows the temperature dependence of (a) the ideality factor (n) and (b) barrier height (ϕ_B) of all samples over the temperature range 200 K to 340 K.
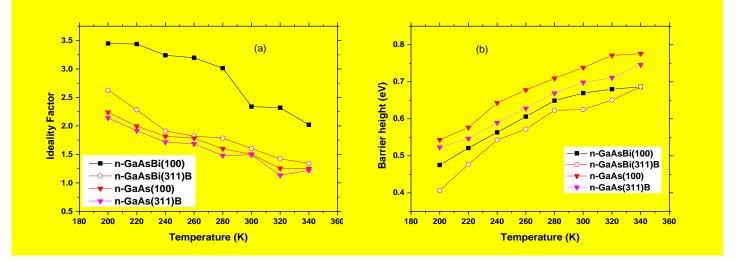

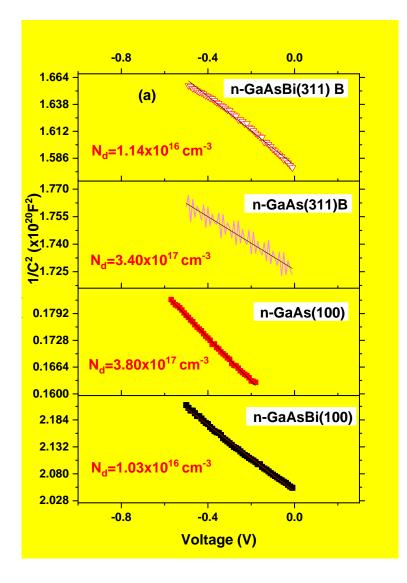Figure 4: Temperature dependence of (a) ideality factor; (b) barrier height, obtained from I-V characterises for all n-type samples.

As can be seen from Table 2, the ideality factor of all devices in forward bias deviates from unity, where n is nearly 2, which suggests that there is significant generation-recombination in depletion region, which is the dominant current mechanism [4,30]. It is worth noting that such deviation of the ideality factor from the thermionic emission can be attributed to several effects, such as inhomogeneity of Schottky barrier height, series resistance, interface states and non-uniformly of interfacial charges [31–33]. As shown in Figure 4 (a) and (b) the values of n decrease with increasing temperature, whereas the values of (ϕ_B) increase as temperature is increased. This behaviour is due to inhomogeneous metal/semiconductor (MS) contacts. At high temperatures, the current flows through the interface states in the regions with a lower barrier height and larger ideality factor, whereas at low temperature the carriers are frozen, and therefore, the current does not follow the thermionic emission mechanism. Note that at low temperature, carriers can overcome the lower barriers, and the transmission mechanism will be dominated by the current flowing through the regions with the lower barrier height. As the temperature increases, the carriers gain enough energy to overcome the higher potential barrier, which causes the barrier height to increase with temperature. As a result, the barrier height will increase, while the ideality factor will decrease with increasing temperatures, due to barrier inhomogeneity in MS contacts [34]. However, (100) GaAsBi has larger ideality factors over all temperatures compared to other diodes, whereas the (311)B GaAs has the smallest values. It is worth noting that, and as to our knowledge, no previous reports have explained the Schottky diodes behaviour in GaAsBi grown on different substrate orientations in the literature. Therefore, the results will be discussed in context with dilute nitride GaAsN instead. Furthermore, from Table 2 it can also be seen that the barrier height at room temperature for (100) GaAsBi and (311)B GaAsBi are reduced compared with reference samples. In particular, (100) GaAs has relatively larger barrier height, while the (311)B GaAsBi diodes have the lowest values. This reduction in barrier height was observed also by Chen et al. [35] in their

study using Cu Schottky contacts to n-type GaAsN grown on (100) and (311)A/B GaAs substrates grown by Chemical beam epitaxy (CBE). They found that samples grown on (311)B exhibited lower barrier height than (100). They attributed this reduction to the polarity of growth surface. On the other hand, Narayanamurti et al. [36] observed in their study using the ballistic electron emission microscopy (BEEM) technique, that the barrier height at room temperature decreases as the nitrogen content increases. They attributed the reduction in the barrier height to the reduction of the band gap, with increasing incorporation of nitrogen. It is well-known that Bi incorporation is more enhanced in (311)B than in (100) GaAs substrates. This results in an enhancement of the reduction of the energy band gap of (311)B with respect to the (100) samples, as reported previously [12,37]. This fact could explain the larger reduction of the barrier height observed in the (311)B samples.

II- Capacitance-Voltage Characteristics

The capacitance – voltage (C-V) measurements were carried out at room temperature with a frequency of 1 MHz in order to determine the free carrier concentration (N_d). Figure 5 (a) shows the experimental net carrier concentration N_d obtained from the slope of $1/C^2$ as a function of V (reverse voltage) for all samples. The free carrier concentration was found to be homogeneous for all samples. In particular, the free carrier concentrations of (100) GaAs, (311)B GaAs, (100) GaAsBi and (311)B GaAsBi , are ~ 3.8×10^{17} cm^{-3} , 3.4×10^{17} cm^{-3}, ~1.03×10^{16} cm^{-3} and ~1.14×10^{16} cm^{-3} , respectively. Figure 5 (b) shows Capacitance/Area (C/A) versus V plot for (100) and (311)B GaAsBi samples. As can be seen from Figure 5 (b), the value of the C/A of sample grown on (311)B has lower C/A than the one grown on (100). This reduction of C/A of (311)B sample could possibly be due to the growth orientation, which was found to affect the shallow donor concentration N_d, as confirmed previously by Hall measurement [35,38,39].
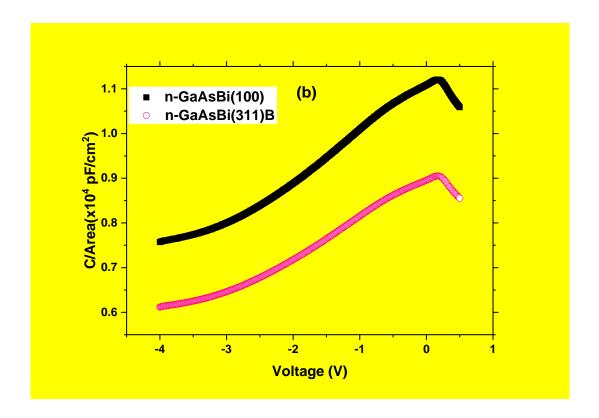
Figure 5: (a) Plot of $1/C^2$ versus reverse bias voltage for n-type (100) GaAs, (311)B GaAs, (100) GaAsBi and (311)B GaAsBi at room temperature. (b) The experimental C/A versus V plot for (100) and (311)B GaAsBi samples at room temperature.

III- DLTS and Laplace (DLTS) Measurements

In order to study the electrically active defects with energies within the forbidden band gap of these n-type (100) GaAs, (311)B GaAs, (100) GaAsBi and (311)B GaAsBi devices, DLTS technique has been employed [40]. As can be seen in Figure 6, the measurements were carried out over a temperature range from 100 K up to 450 K. The experimental parameters used are: reverse bias (V_R) of -1 V, filling pulse voltage (V_P) of 0V with filling pulse time (tp) of 1 msec and rate window set to be at 200 s^{-1} for all investigated samples.
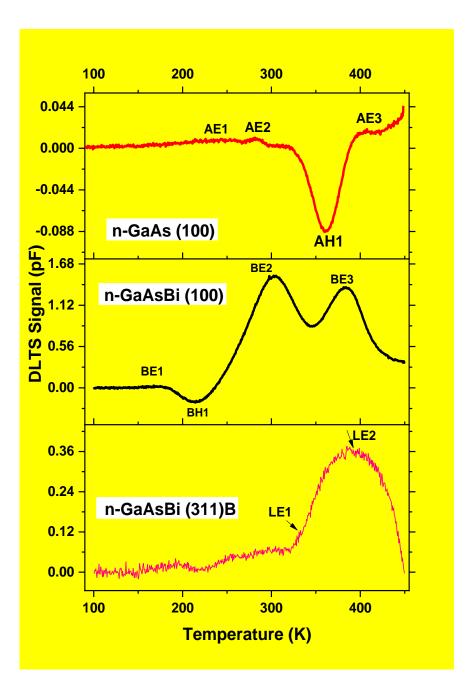
Figure 6: Typical DLTS spectra scans for n-type (100) GaAs, (100) GaAsBi and (311)B GaAsBi samples.

The standard DLTS spectra in Figure 6 of (100) GaAs and (100) GaAsBi samples show three positive peaks corresponding to three majority electron traps. In addition to the electron traps, a hole traps (negative peaks) were also observed in (100) GaAsBi and (100) GaAs, respectively. While for GaAsBi sample grown on (311)B (Figure 6), a very broad peak is detected over the temperature range ~ 325 K to ~450 K. For control sample (311)B GaAs no

defects were detected by DLTS as their concentrations could be too low and are outside the detection limit of DLTS. In order to resolve the broad peaks obtained by DLTS measurements, as well for a better resolution of DLTS spectra observed in the investigated samples, Laplace DLTS (LDLTS) measurements were performed [41] on all samples, under same conditions as those used in DLTS experiments. Laplace DLTS revealed the presence of the following traps: (i) (100) GaAs and (100) GaAsBi: three electron traps labelled as (AE1, AE2 and AE3) and (BE1, BE2 and BE3), one hole trap (AH1) and (BH1), respectively; (ii) (311)B GaAsBi: two electron traps namely (LE1 and LE2). The activation energies of each defect were determined from the Arrhenius plot of the emission rates as a function of inverse temperature as illustrated in Figure 7.
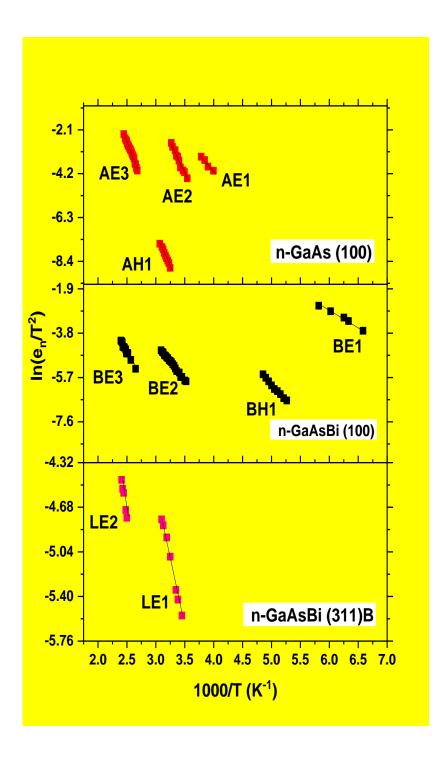
Figure 7: Arrhenius plots obtained from Laplace DLTS for n-GaAsBi grown on (a) (100) and, (b) (311)B GaAs substrate, with reverse voltage V_R=-1, filling pulse height V_p=0V, and filling pulse time t_p=1 msec.

The traps activation energies, apparent cross section and trap concentrations are calculated from the slope and intercept of the Arrhenius plot. The traps parameters are summarised in Table 3.

Table 3: Traps parameters for n-(100) GaAs and n- (100) GaAsBi and (311)B GaAsBi.

Sample	Trap Label	Activation energy (eV)	Apparent capture cross-section (cm^2)	Trap concentration (cm^{-3})
n-GaAs (100)	AE1	0.28±0.03	4.3x10^{-17}	8.2x10^{15}
	AE2	0.54±0.02	2.1x10^{-13}	7.2x10^{15}
	AH1	0.53±0.02	4.8x10^{-16}	8.1x10^{15}
	AE3	0.61±0.01	1.8x10^{-14}	5.1x10^{15}
n-GaAsBi (100)	BE1	0.12±0.01	1.1x10^{-18}	1.2x10^{13}
	BH1	0.24±0.01	9.8x10^{-18}	5.1x10^{13}
	BE2	0.27±0.01	9.3x10^{-19}	7.7x10^{14}
	BE3	0.41±0.04	6.3x10^{-18}	9.7x10^{14}
n-GaAsBi (311)B	LE1	0.19±0.01	5.1x10^{-20}	1.4x10^{13}
	LE2	0.29±0.01	1.8x10^{-19}	1.9x10^{14}

It can be seen from Table 3, that the number of traps detected in sample grown on (100) are higher than sample grown on (311)B. In fact, R. Mari [26] observed that the substrate orientations of GaAs have a significant impact on the incorporation of impurities and traps into the structure. It was reported that impurities are more susceptible to be incorporated in (100) plane than in other high index planes. This result correlated with I-V characterization discussed

above, where sample grown on (100) has higher reverse current than sample grown on (311)B due to higher number of traps.

The best way to identify these active traps created as a result of substrate orientations are to compare their activation energies to each other and/or their DLTS signals. The obtained results are also discussed and compared with previous works.

The traps BE1 (0.12±0.01eV) and LE1 (0.19±0.01) observed in (100) GaAsBi and (311)B GaAsBi, respectively, are likely to correspond to the same traps ET_0 and ET_1 with activation energies ranging from 0.07 to 0.19eV [7] and A' with activation energy of 0.12 eV [11] reported previously. These were assigned to traps involving Bi as a constituent.

Traps AE1, BE2, and LE2 with similar activation energies in the range 0.27 to 0.29eV could be of the same origin. This trap, labelled as ET_2 with an activation energy in the range 0.29 to 0.33eV, was observed also in both GaAs and GaAsBi grown by MBE at low temperature by Gelczuk et al. [7]. This deep level can be attributed to the well-known M_3 trap (E_c-0.34 eV) [42,43] , which has same signature as EL6 trap reported in ref.[43]. The EL6 trap is generally related to complex pair defects involving arsenic antisite (As_{Ga}) and arsenic vacancy (V_{As}) [43] or to divacancy complex defect (V_{Ga} - V_{As}) [44]. On the other hand, using theoretical calculations by density functional theory (DFT method) [45] a trap with energy of 0.36 eV (similar to BE2) was found. The authors attributed its origin to a complex defect involving Bi.

Furthermore, the traps AE2 and BE3 with activation energies 0.54±0.02 eV and 0.41±0.04 eV and trap concentrations of 7.2×10^{15} cm^{-3} and 9.7×10^{14} cm^{-3}, were observed only in n-type (100) GaAs and GaAsBi samples, respectively. Similar deep defect was detected in n-type GaAsBi samples grown at temperatures 330℃ and 390℃, respectively , labelled as trap C [11] and trap ET3 [7] with activation energies varying in the range from 0.45 to 0.52 eV [7] . This trap most

likely correspond to the trap level M4. The origin of this trap was attributed to an arsenic vacancy (V_{As}) complex involving an impurity [46].

 In addition, the trap level AE3 with activation energy of 0.61±0.01 eV and concentration 5.1×10^{15} cm^{-3} was detected only in the n- (100) GaAs control sample (without Bi). This trap was observed also in GaAs and GaAsBi as the dominant electron trap [7]. It was suggested that the origin of this deep level trap could possibly be attributed to trap M6, whose activation energy is (0.62 eV) [47]. It is interesting to note that M6 trap is a unique trap in GaAs layers grown by MBE [42]. The origin of this trap might be related to gallium and arsenic vacancies (V_{As} - V_{Ga}) or impurity related complexes (V_{As} – X- V_{Ga}), where X refers to the impurity or interstitial [47]

 As seen in Table 3, hole traps were also observed in (100) GaAs and (100) GaAsBi labelled as (AH1) and (BH1), with activation energies (0.53±0.02) eV, (0.24±0.01) eV, respectively. Minority hole trap AH1 appears to have a similar activation energy as that of trap H2 [48], and the trap with activation 0.54±0.02 eV observed in ref.[49]. This trap was suggested to be likely attributed to donor level of the arsenic antisite As_{Ga} complexes defect [48]. Trap BH1 has similar DLTS spectra as those observed in p- type GaAsBi grown by MBE [50] and labelled as HT2 and HT3 with activation energies over a range (0.23- 0.43eV). These traps were assigned to As_{Ga} or its relevant cluster.

3.3- Optical Properties
IV- Raman Spectroscopy

Figure 8 shows the Raman spectra for all samples, i.e., (100) GaAs and (311)B GaAs (control samples) and (100) GaAsBi and (311)B GaAsBi, in the ranges (i) 150 to 245 cm^{-1} and (ii) 250 to 300 cm^{-1}.

Two intense peaks in the range of 260-300 cm^{-1} were observed in all samples. These Raman peaks are associated with the GaAs optical phonons at the Brillouin zone centre [51,52]. Particularly, the transverse optical mode (TO(Γ)) is observed at around 267 cm^{-1} and the longitudinal optical mode (LO(Γ)) at around 291 cm^{-1}. Furthermore, the GaAs TO (Γ) Raman peak is forbidden by Raman selection rules for the (100) samples , while for the (311)B samples this peak is allowed [53,54]. A broad TO (Γ) Raman peak was observed for the (100) GaAsBi sample, which can be explained by a breakdown of Raman selection rules due to Bi-induced disorder.
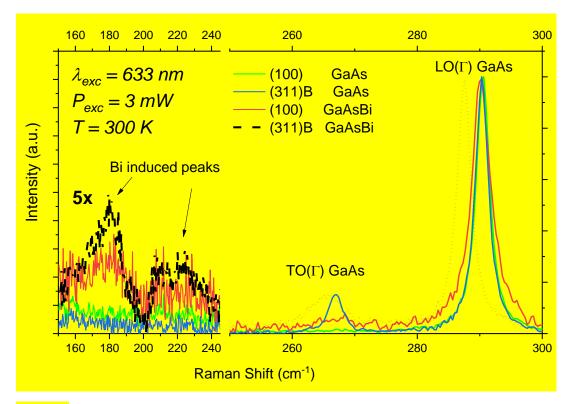

Figure 8: Raman spectra of GaAs and GaAsBi samples grown on GaAs (100) and GaAs (311)B substrates at 300K.

For the GaAsBi samples, additional Raman peaks were detected in the range 150 – 240 cm^{-1}. The observation of these peaks was reported previously for GaAsBi samples [54–60]. Although the nature of the peaks is not well established, it is well known that these peaks are Bi-induced. Our Raman spectra in the range 250 to 300 cm^{-1} were well fitted by two Lorentz functions (the fitting parameters are shown in Table 4). Although these samples are doped, we have observed

no evidence of the presence of the peak due to plasmons-phonons coupling (LOCP). In general, our results show that the contribution of the LOCP is probably small and that this peak is not well resolved from GaAs LO (Γ) and TO (Γ) Raman modes. In addition, a red-shift of the LO (Γ) Raman peak for GaAsBi samples was observed as compared to the reference GaAs samples. It is expected that the incorporation of bismuth atoms will result in significant changes of the mechanical properties of GaAs$_{(1-x)}$Bi$_x$ alloys. Particularly, the Bi incorporation will change the frequency of phonon vibration modes of the crystalline matrix. It was previously observed that the GaAs LO(Γ) position changes linearly with the Bi concentration (x) [54,61]. On the other hand, the phonon frequencies can also be dependent on the presence of strain in the alloys [54,61]. Such stress-induced shifts can basically be described by the phonon deformation potentials (PDPs). Therefore, the total frequency shift could be associated with two different contributions: (i) the changes in the alloying composition (x) of the ternary material ($\Delta\omega_{alloy}$) and (ii) changes of the strain field in the alloy ($\Delta\omega_{strain}$). The total shift of the optical phonon modes can then be quantitatively expressed as $\Delta\omega = \Delta\omega_{strain} + \Delta\omega_{alloy}$ [54,61]. As the Bi content is 5.4% for both (100) and (311)B samples, the different shifts observed for the Raman modes must be due to the strain effect. Particularly for the (311)B sample, the observed shift is - 60 cm^{-1}/xBi which is consistent with previous works [16,55,56,60,61]. On the other hand, for the (100) GaAsBi sample a lower shift was observed probably due to a blue-shift originated by compressive strain (-$\Delta\omega_{strain}$), in agreement with the shift reported by E. Tisbi et al [55]. Furthermore, the HR-XRD results have shown that the strain for the (100) GaAsBi sample is 2.7 times higher than that of (311)B sample. In addition, a broadening of the LO (Γ) Raman peak was observed for the GaAsBi samples, a disordering effect for these samples which is particularly higher in the (100) GaAsBi sample. Similar broadening was also observed for the TO (Γ) Raman mode, but more important the observation of this peak in (100) GaAsBi sample is probably due to Bi induced disorder. A smaller red-

shift of the TO (Γ) Raman peak was observed as compared to the red-shift observed for the LO (Γ) Raman peak for GaAsBi samples, which were similarly reported previously in the literature. In general, our results indicate that the introduction of Bi in the (100) samples results in a higher compressive strain and higher crystal disorder as compared to the GaAsBi (311)B samples. These differences have an important impact on the optical emission of these samples as will be discussed below.

Table 4: Lorentzian fitting parameters:

	(100)	(100)	(311)B	(311)B
LO(Γ)				
ω_{peak} (cm^{-1})	290.5	290.2	290.3	287.5
FWHM $-\Delta\omega$ (cm^{-1})	2.6	3.7	2.5	2.8
Peak relative intensity	1.00	0.98	1.00	0.97
TO(Γ)				
ω_{peak} (cm^{-1})	262.4	266.7	266.9	265.5
FWHM $-\Delta\omega$ (cm^{-1})	22.9	10.6	2.7	6.7
Peak relative intensity	0.007*	0.04	0.16	0.13
Reduced chi-square	2.59 10^{-5}	1.77 10^{-4}	3.26 10^{-5}	9.14 10^{-5}
Residual Sum of Squares	0.00411	0.02807	0.00518	0.01453
R-Square	0.9992	0.9957	0.9990	0.9971

* less than the noise level ≈ 0.01
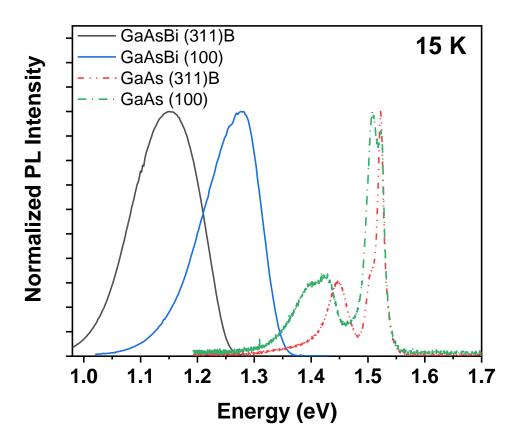
V- Photoluminescence

Figure 9: Normalized PL spectra of GaAs and GaAsBi layers at 15K

Figure 9 shows the photoluminescence spectra of GaAs (100), GaAs (311) B, GaAsBi (100) and GaAsBi (311)B layers. A sharp emission is clearly seen at around 1.52eV for both GaAs layers as expected. In addition, other PL peaks were also observed: one around 1.508 eV and a broad band in the range of 1.3-.49 eV which were mainly associated to transitions related to GaAs –like traps/impurities due to the growth conditions. On the other hand, the PL spectra of both (100) and (311)B $GaAs_{0.94}Bi_{0.05}$ layers show a redshift as compared to GaAs samples, as expected [62–64]. The observed redshift of PL peak position was associated with Bi incorporation which induces a band gap reduction. Although both samples have the same Bi

concentration, we have observed that the PL peak position of both samples are different and do not show the standard red shift of 89 meV/Bi% previously reported in the literature for GaAsBi layers [1,62,64]. Actually, for our samples this red shift is lower than previously reported. This effect is particularly more important for the (100) GaAsBi sample. It was previously shown a similar behavior for n-doped (100) GaAsBi samples [7] which was associated with the contribution of Bi induced donor traps next to the conduction band which could also induce an additional emission in the spectrum due to a donor traps (DT)-valence band (VB) transition and therefore could result in a reduced red shift . Particularly, our results show that the PL red shift of (100) GaAsBi layer is much lower than for (311)B GaAsBi sample although both samples have the same Bi concentration of 5.4 %. The obtained values of PL peak position for the (100) and (311)B samples are different and could be due to the other contributions such as different Bi induced traps in these samples. However, the XRD results for these samples show that the samples also have different strain which could affect considerably their optical properties. Particularly, we notice that the DLTS results have shown higher number of carrier traps for the (100) GaAsBi sample as compared to the (311)B GaAsBi sample which certainly could affect significantly its optical properties. However, the XRD results have also shown that the compressive strain for the (100) sample is 2.7 times higher than for the (311) B sample. An increase of compressive strain will certainly result in important changes in the band structure resulting in blue shift of PL peak position as shown previously [55].
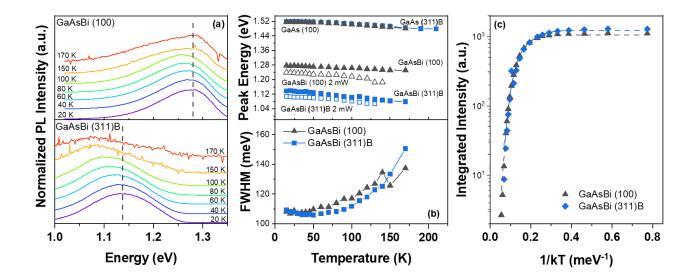
Figure 10: Temperature dependence of (a) PL spectra and of (b) PL peak position and linewidth (c) Arrhenius Plot and activation energies for (100) and (311)B GaAsBi samples.

Figure 10 (a) shows the temperature dependence of the PL spectra, peak energy and FWHM of the doped $GaAs_{(1-x)}Bi_x$ samples. We observed that the PL energy peaks (Figure 10 (b)) exhibit a monotonic redshift with increasing temperature due to the decrease of the band-gap energy with increasing temperature as expected. We have analyzed the temperature dependence of PL intensity with a modified Arrhenius equation [15]:

$$\frac{I_{PL}(T)}{I_0} = \frac{1}{1 + A_1 e^{\frac{-E_1}{k_B T}} + A_2 e^{\frac{-E_2}{k_B T}}}$$

where I_{PL} is the integrated PL intensity, A_1 and A_2 are constants related to the density of non-radiative recombination centers, E_1 and E_2 are activation energies, k_B is the Boltzmann constant, T the temperature and I_0 the approximate PL intensity when T→0. Figure 10(c) shows the obtained results of Arrhenius fitting and the activation energy values for both GaAsBi (100) and (311)B samples. The obtained E1 and E2 values for (100) and (311)B

samples are 20meV and 95meV, and 28 mV and 74 meV, respectively. These values evidence the presence of Bi clusters and alloy disorder in both samples. Actually, it was previously reported that the $GaAs_{(1-x)}Bi_x$ layers usually have localized Bi pairs and clusters, which have different configurations and binding energies, and also alloy disorder, and potential fluctuation [15]. Particularly, it was previously reported that the presence of defects/disorder results in two different activation energies: one in the range of 8–17 meV which is usually related to Bi clusters and Bi pairs and another around 50 meV which is usually related to GaAsBi alloy disorder [15,65]. Therefore our experimental values are fully consistent to this interpretation.
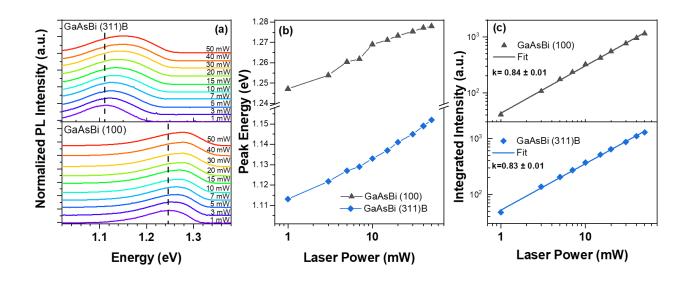

Figure 11: (a) PL spectra for different laser power (b) PL peak position and (c) Double logarithmic plot of the integrated intensity as function of laser power for GaAsBi (100) and (311)B samples at 10K.

The laser power dependence of PL spectra for both samples was also investigated. Figure 11 (a), (b) and (c) shows the PL spectra versus laser power, the laser power dependence of PL peak position, and integrated PL, respectively at 10K. We observed that there is a clear blue shift of PL peak energy with increasing laser power. However, this effect seems to be different for (311)B and (100) GaAsBi samples. Particularly, for the (100) samples we have observed

a blue shift of about 25meV with increasing laser power, while for the (311)B sample we have observed a blue shift of about 43meV for a laser power of 50mW (Figure 11(a) and (b)). Figure 11(c) shows the laser power dependence of integrated PL intensity also at 10K. The laser power dependence was fitted by using the power law which is a standard procedure to investigate the nature of the PL band in semiconductor materials and is given by the following expression: $I = \alpha (P)^k$, where I is the integrated PL intensity, P is the laser power, α and k are fitting parameters [15,62]. It is well known for free exciton emission it is expected to obtain $k \approx 1$ [15,62]. However, for our samples we have obtained a value slightly lower than k=1, i.e., $k \approx 0.8$ for the higher laser power range of 1-50mW. Our results indicate some exciton localization which is similar to several previous results reported in the literature for GaAsBi layers [15,62,65]. Therefore, we have associated our results with the emission of localized excitons by the presence of Bi clusters/ alloy disorder, which manifests in a clear blue shift of the PL peak with increasing laser power and is consistent with the obtained values for E_1 and E_2 activation energies [15,62,65]. We also remark that the DLTS results for the (100) sample have shown a larger number of traps as compared to the (311)B sample. As mention above, it was previously reported for n-doped (100) GaAsBi sample that the PL spectra have also a contribution of optical transition related to Bi induced traps close to the conduction band (donor band) which could also affect the laser power dependence and the PL peak position [7]. Therefore, our PL results are consistent with the DLTS results of these samples that have shown that the number of Bi induced traps are more important for (100) GaAsBi samples and therefore these traps affect more the PL of (100) samples as compared with the (311)B sample. On the other hand, as mentioned previously the higher compressive strain observed for (100) GaAsBi sample could also affect its optical properties resulting in the observation of PL peak position at higher energy as compared to GaAsBi (311)B sample with the same amount of Bi%.

4- Conclusion

We have investigated structural, electrical and optical properties of n-type GaBiAs layers grown under similar conditions on GaAs (100) and (311)B planes . It was found that although these samples have the same Bi concentration of 5.4%, they have shown different compressive strain which has important impact on their optical properties. Furthermore, it was observed that the introduction of Bi reduces the GaAs like electron traps but also induces Bi-related donor traps which are different for GaAsBi samples grown on (100) and (311)B planes. Particularly, the DLTS results have shown that Bi traps are reduced considerably for (311)B samples. Finally, the observed differences in the optical properties of (100) and (311)B GaAsBi samples can be explained by the presence of different compressive strain and by the presence of Bi-induced traps which affect considerably the optical properties of GaAsBi layers.

References:

[1]   S. Francoeur, M.-J. Seong, A. Mascarenhas, S. Tixier, M. Adamcyk, T. Tiedje, *Band gap of GaAs1−xBix, 0<x<3.6%*, Appl. Phys. Lett. **82**, 3874 (2003).

[2]   B. Fluegel, S. Francoeur, A. Mascarenhas, S. Tixier, E.C. Young, T. Tiedje, *Giant spin-orbit bowing in GaAs1-xBix*, Phys. Rev. Lett. **97**, 067205 (2006).

[3]   Z. Batool, K. Hild, T.J.C. Hosea, X. Lu, T. Tiedje, S.J. Sweeney, *The electronic band structure of GaBiAs/GaAs layers: Influence of strain and band anti-crossing*, J. Appl. Phys. **111**, 11310 (2012).

[4]   Z. Zhou, D.F. Mendes, R.D. Richards, F. Bastiman, J.P. David, *Absorption properties of GaAsBi based p–i–n heterojunction diodes*, Semicond. Sci. Technol. **30**, 094004 (2015).

[5]   V. Pačebutas, K. Bertulis, G. Aleksejenko, A. Krotkus, *Molecular-beam-epitaxy grown GaBiAs for terahertz optoelectronic applications*, J. Mater. Sci. Mater. Electron. **20**, 363 (2009).

[6]   X. Lu, D.A. Beaton, R.B. Lewis, T. Tiedje, M.B. Whitwick, *Effect of molecular beam epitaxy growth conditions on the Bi content of GaAs1−xBix*, Appl. Phys. Lett. **92**, 192110 (2008).

[7]   Ł. Gelczuk, J. Kopaczek, T.B.O. Rockett, R.D. Richards, R. Kudrawiec, *Deep-level defects in n-type GaAsBi alloys grown by molecular beam epitaxy at low temperature and their influence on optical properties*, Sci. Rep. **7**, 12824 (2017).

[8]   A.R. Mohmad, F. Bastiman, C.J. Hunter, J.S. Ng, S.J. Sweeney, J.P.R. David, *The effect of Bi composition to the optical quality of GaAs 1−x Bi x*, Appl. Phys. Lett. **99**, 042107 (2011).

[9]   J. Gebauer, R. Krause-Rehberg, S. Eichler, M. Luysberg, H. Sohn, E.R. Weber, *Ga vacancies in low-temperature-grown GaAs identified by slow positrons*, Appl. Phys. Lett. **71**, 638 (1997).

[10]   P.M. Mooney, M.C. Tarun, V. Bahrami-Yekta, T. Tiedje, R.B. Lewis, M. Masnadi-Shirazi, *Defect energy levels in p-type GaAsBi and GaAs grown by MBE at low temperatures*, Semicond. Sci. Technol. **31**, 065007 (2016).

[11]   P.M. Mooney, K.P. Watkins, Z. Jiang, A.F. Basile, R.B. Lewis, V. Bahrami-Yekta, M. Masnadi-Shirazi, D.A. Beaton, T. Tiedje, *Deep level defects in n-type GaAsBi and GaAs grown at low temperatures*, J. Appl. Phys. **113**, 13370 (2013).

[12]   M. Henini, J. Ibáñez, M. Schmidbauer, M. Shafi, S. V. Novikov, L. Turyanska, S.I. Molina, D.L. Sales, M.F. Chisholm, J. Misiewicz, *Molecular beam epitaxy of GaBiAs on (311) B GaAs substrates*, Appl. Phys. Lett. **91**, 350 (2007).

[13]   J.F. Rodrigo, D.L. Sales, M. Shafi, M. Henini, L. Turyanska, S. Novikov, S.I. Molina, *Effect of annealing on the structural and optical properties of (3 1 1)B GaAsBi layers*, Appl. Surf. Sci. **256**, 5688 (2010).

[14]   P.K. Patil, F. Ishikawa, S. Shimomura, *GaAsBi/GaAs MQWs MBE growth on (411) GaAs substrate*, Superlattices Microstruct. **100**, 1205 (2016).

[15]   G.A. Prando, V. Orsi Gordo, J. Puustinen, J. Hilska, H.M. Alghamdi, G. Som, M. Gunes, M. Akyol, S. Souto, A.D. Rodrigues, H.V.A. Galeti, M. Henini, Y.G. Gobato, M. Guina, *Exciton localization and structural disorder of GaAs1-xBix/GaAs quantum wells grown by molecular beam epitaxy on (311)B GaAs substrates*, Semicond. Sci. Technol. **33**, 084002 (2018).

[16]   J.A. Steele, R.A. Lewis, M. Henini, O.M. Lemine, A. Alkaoud, *Raman scattering studies*

of strain effects in (100) and (311)B GaAs 1-xBix epitaxial layers, J. Appl. Phys. **114**, 193516 (2013).

[17] R.N. Kini, L. Bhusal, A.J. Ptak, R. France, A. Mascarenhas, *Electron Hall mobility in GaAsBi*, J. Appl. Phys. **106**, 04370 (2009).

[18] R.L. Field, J. Occena, T. Jen, D. Del Gaudio, B. Yarlagadda, C. Kurdak, R.S. Goldman, *Influence of surface reconstruction on dopant incorporation and transport properties of GaAs(Bi) alloys*, Appl. Phys. Lett. **109** (2016) 252105.

[19] M. Yoshimoto, M. Itoh, Y. Tominaga, K. Oe, *Quantitative estimation of density of Bi-induced localized states in GaAs1−xBix grown by molecular beam epitaxy*, J. Cryst. Growth. **378**, 73 (2013).

[20] M.A. Stevens, S. Lenney, J. McElearney, K.A. Grossklaus, T.E. Vandervelde, *Characterization of tellurium and silicon as n-type dopants for GaAsBi*, Semicond. Sci. Technol. **35**, 105006 (2020).

[21] B.A. Aronzon, M. V. Kovalchuk, E.M. Pashaev, M.A. Chuev, V. V. Kvardakov, I.A. Subbotin, V. V. Rylkov, M.A. Pankov, I.A. Likhachev, B.N. Zvonkov, Y.A. Danilov, O. V. Vihrova, A. V. Lashkul, R. Laiho, *Structural and transport properties of GaAs/δ-Mn/GaAs/In xGa1-xAs/GaAs quantum wells*, J. Phys. Condens. Matter. **20**, 145207 (2008).

[22] D.K. Bowen, B.K. Tanner, *High Resolution X-Ray Diffractometry And Topography*, (CRC Press, 2005).

[23] L. Vegard, *Die Konstitution Der Mischkristalle Und Die Raumfüllung Der Atome*, Zeitschrift Für Phys. **5**, 17 (1921).

[24] M. Ferhat, A. Zaoui, *Structural and electronic properties of III-V bismuth compounds*,

Phys. Rev. B. **73**, 115107 (2006).

[25] R.H. Mari, M. Shafi, M. Henini, D.Taylor, *Laplace DLTS of molecular beam epitaxy GaAs grown on (100) and (211)B substrates*, Phys. Status Solidi. **12**, 2873 (2009).

[26] R.H. Mary, *Electrical characterisation of defects in III-V compound semiconductors by DLTS*, 2011.

[27] S.M. Sze, K.K. Ng, *Physics of Semiconductor Devices*, John Wiley & Sons, 2006.

[28] M. Biber, C. Coşkun, A. Türüt, *Current-voltage-temperature analysis of inhomogeneous Au/n-GaAs Schottky contacts*, Eur. Phys. J. Appl. Phys. **31**, 79–86 (2005).

[29] J.H. Werner, *Schottky barrier and pn-junctionI/V plots-Small signal evaluation*, Appl. Phys. A. **47**, 291 (1988).

[30] C.J. Hunter, F. Bastiman, A.R. Mohmad, R. Richards, J.S. Ng, S.J. Sweeney, J.P.R. David, *Absorption characteristics of GaAs1-xBix/GaAs Diodes in the Near-Infrared*, IEEE Photonics Technol. Lett. **24**, 2191 (2012).

[31] B. Şahin, H. Çetin, E. Ayyildiz, *The effect of series resistance on capacitance–voltage characteristics of Schottky barrier diodes*, Solid State Commun. **135**, 490 (2000).

[32] E.H. Rhoderick, *Metal-semiconductor contacts*, IEE Proc. I-Solid-State Electron Devices. **129** (1982).

[33] N. Al Saqri, J.F. Felix, M. Aziz, D. Jameel, C.I.L. de Araujo, H. Albalawi, F. Al Mashary, H. Alghamdi, D. Taylor, M. Henini, *Investigation of the effects of gamma radiation on the electrical properties of dilute GaAs1−xNx layers grown by Molecular Beam Epitaxy*, Curr. Appl. Phys. **15** (2015).

[34]   N. Yildirim, H. Korkut, A. Türüt, *Temperature-dependent Schottky barrier inhomogeneity of Ni/n-GaAs diodes*, Eur. Phys. J. Appl. Phys. **45**, 10302 (2009).

[35]   C. Dong, X. Han, X. Gao, Y. Ohshita, M. Yamaguchi, *Electrical characterization of Cu Schottky contacts to n-type GaAsN grown on (311)A/B GaAs substrates*, J. Alloys Compd. **657** (2016).

[36]   V. Narayanamurti, M. Kozhevnikov, H.P. Xin, C.W. Tu, A. Mascarenhas, Y. Zhang, *Nitrogen-induced evolution of GaAs 1-x N x studied by ballistic electron emission spectroscopy*, Natl. Renew. Energy Lab.(NREL). (2000).

[37]   R. Kudrawiec, P. Poloczek, J. Misiewicz, M. Shafi, J. Ibáñez, R.H. Mari, M. Henini, M. Schmidbauer, S.V. Novikov, L. Turyanska, S.I. Molina, D.L. Sales, M.F. Chisholm, *Photomodulated transmittance of GaBiAs layers grown on (001) and (311)B GaAs substrates*, Microelectronics J. **40** (2009).

[38]   J.V.V.N.K. Rao, S.V. Reddy, S.S. Naik, *Electrical Characteristics of Rapid Thermal Annealing Effects on Co-polymer of Au / P (VDC-MA) / n-type InP Schottky Structures*, Int. J. Res. Stud. Sci. Eng. Technol. **3** (2016).

[39]   X. Han, C. Dong, Q. Feng, Y. Ohshita, M. Yamaguchi, *Growth orientation dependence of Si doping in GaAsN*, J. Appl. Phys. **117**, 05570 (2015).

[40]   D. V. Lang, *Deep-level transient spectroscopy: A new method to characterize traps in semiconductors*, J. Appl. Phys. **45**, 3023 (1974).

[41]   L. Dobaczewski, A.R. Peaker, K. Bonde Nielsen, *Laplace-transform deep-level spectroscopy: The technique and its applications to the study of point defects in semiconductors*, J. Appl. Phys. **96**, 4689 (2004).

[42]   D. V. Lang, A.Y. Cho, A.C. Gossard, M. Ilegems, W. Wiegmann, *Study of electron traps*

in n -GaAs grown by molecular beam epitaxy, J. Appl. Phys. **47**, 2558 (1976).

[43] K. Yokota, H. Kuchii, K. Nakamura, M. Sakaguchi, H. Takano, Y. Ando, *EL2, EL3, and EL6 defects in GaAs highly implanted with sulfur*, J. Appl. Phys. **88**, 5017 (2000).

[44] Z.Q. Fang, T.E. Schlesinger, A.G. Milnes, *Evidence for EL6 (Ec- 0.35 eV) acting as a dominant recombination center in n-type horizontal Bridgman GaAs*, J. Appl. Phys. **61**, 5047 (1987).

[45] G. Luo, S. Yang, G.R. Jenness, Z. Song, T.F. Kuech, D. Morgan, *Understanding and reducing deleterious defects in the metastable alloy GaAsBi*, NPG Asia Mater. **9** (2017).

[46] P. Blood, J.J. Harris, *Deep states in GaAs grown by molecular beam epitaxy*, J. Appl. Phys. **56**, 993 (1984).

[47] A.Z. Li, H.K. Kim, J.C. Jeong, D. Wong, T.E. Schlesinger, A.G. Milnes, *Trap suppression by isoelectronic In or Sb doping in Si-doped n -GaAs grown by molecular-beam epitaxy*, J. Appl. Phys. **64**, 3497 (1988).

[48] P.M. Mooney, M. Tarun, D.A. Beaton, A. Mascarenhas, K. Alberi, *Deep level defects in dilute GaAsBi alloys grown under intense UV illumination*, Semicond. Sci. Technol. **31**, 085014 (2016).

[49] J. Lagowski, D.G. Lin, T. -P. Chen, M. Skowronski, H.C. Gatos, *Native hole trap in bulk GaAs and its association with the double-charge state of the arsenic antisite defect*, Appl. Phys. Lett. **47**, 929 (1985).

[50] T. Fuyuki, S. Kashiyama, Y. Tominaga, K. Oe, M. Yoshimoto, *Deep-hole traps in p-type GaAs1-xBix grown by molecular beam epitaxy*, Jpn. J. Appl. Phys. **50**, 080203 (2011).

[51] R. Loudon, *The Raman effect in crystals*, Adv. Phys. **13**, 423 (1964).

[52] R. Merlin, A. Pinczuk, W.H. Weber, *Overview of Phonon Raman Scattering in Solids, in Raman Scattering in Materials Science*, edited by R. Merlin and W. H. Weber, Springer, New York. (2000).

[53] J.A. Steele, P. Puech, and R.A. Lewis, *Polarized Raman backscattering selection rules for (hhl)-oriented diamond- and zincblende-type crystals*, J. Appl. Phys. **120**, 05570 (2016).

[54] J. A. Steele, *Structural and Optical Studies of GaAs1-XBix and p-Bi203 for Optoelectronic Devices*, University of Wollongong, 2015 and references therein.

[55] E. Tisbi, E. Placidi, R. Magri, P. Prosposito, R. Francini, A. Zaganelli, S. Cecchi, E. Zallo, R. Calarco, E. Luna, J. Honolka, M. Vondráček, S. Colonna, F. Arciprete, *Increasing Optical Efficiency in the Telecommunication Bands of Strain-Engineered Ga(As,Bi) Alloys*, Phys. Rev. Appl. **14**, 014028 (2020).

[56] P. Verma, K. Oe, M. Yamada, H. Harima, M. Herms, G. Irmer, *Raman Studies on GaAs1−xBi x and InAs1−xBix*, J. Appl. Phys. **89**, 1657 (2001).

[57] M.J. Seong, S. Francoeur, S. Yoon, A. Mascarenhas, S. Tixier, M. Adamcyk, T. Tiedje, *Bi-induced vibrational modes in GaAsBi*, Superlattices Microstruct. **37**, 394 (2005).

[58] F. Sarcan, Ö. Dönmez, K. Kara, A. Erol, E. Akalın, M. Çetin Arıkan, H. Makhloufi, A. Arnoult, C. Fontaine, *Bismuth-induced effects on optical, lattice vibrational, and structural properties of bulk GaAsBi alloys*, Nanoscale Res. Lett. **9**, 119 (2014).

[59] R.S. Joshya, V. Rajaji, C. Narayana, A. Mascarenhas, R.N. Kini, *Anharmonicity in light scattering by optical phonons in GaAs1-xBix*, J. Appl. Phys. **119**, 20570 (2016).

[60] J. Li, K. Forghani, Y. Guan, W. Jiao, W. Kong, K. Collar, T.H. Kim, T.F. Kuech, and A.S. Brown, *GaAs1-yBiy Raman signatures: Illuminating relationships between the*

electrical and optical properties of GaAs1-yBiy and Bi incorporation, AIP Adv. **5**, 067103 (2015).

[61] A. Erol, E. Akalin, K. Kara, M. Aslan, V. Bahrami-Yekta, R.B. Lewis, T. Tiedje, *Raman and AFM studies on nominally undoped, p- and n-type GaAsBi alloys*, J. Alloys Compd. **722**, 339 (2017).

[62] R. Kudrawiec, M. Syperek, P. Poloczek, J. Misiewicz, R.H. Mari, M. Shafi, M. Henini, Y.G. Gobato, S. V. Novikov, J. Ibáñez, M. Schmidbauer, S.I. Molina, *Carrier localization in GaBiAs probed by photomodulated transmittance and photoluminescence*, J. Appl. Phys. **106**, 02351 (2009).

[63] M. Usman, C.A. Broderick, A. Lindsay, E.P. O'Reilly, *Tight-binding analysis of the electronic structure of dilute bismide alloys of GaP and GaAs*, Phys. Rev. B - Condens. Matter Mater. Phys. **84**, 245202 (2011).

[64] O.M. Lemine, A. Alkaoud, H. V. Avanço Galeti, V. Orsi Gordo, Y. Galvão Gobato, H. Bouzid, A. Hajry, M. Henini, *Thermal annealing effects on the optical and structural properties of (1 0 0) GaAs1-xBix layers grown by Molecular Beam Epitaxy*, Superlattices Microstruct. **65**, 48 (2014).

[65] S. Mazzucato, P. Boonpeng, H. Carrère, D. Lagarde, A. Arnoult, G. Lacoste, T. Zhang, A. Balocchi, T. Amand, X. Marie, C. Fontaine, *Reduction of defect density by rapid thermal annealing in GaAsBi studied by time-resolved photoluminescence*, Semicond. Sci. Technol. **28**, 022001 (2013).